

---



---

OPTICAL  
PROPERTIES

---



---

## A PL and PLE Study of High Cu Content $\text{Cu}_2\text{ZnSnSe}_4$ Films on Mo/Glass and Solar Cells

M. A. Sulimov<sup>a, b, \*</sup>, M. V. Yakushev<sup>a, b, c</sup>, I. Forbes<sup>d</sup>, J. M. Prieto<sup>d</sup>, A. V. Mudryi<sup>e</sup>,  
Ju. Krustok<sup>f</sup>, P. R. Edwards<sup>g</sup>, and R. W. Martin<sup>g</sup>

<sup>a</sup> *Mikheev Institute of Metal Physics, Ural Branch, Russian Academy of Sciences, Yekaterinburg, Russia*

<sup>b</sup> *Ural Federal University Named after the First President of Russia B.N. Yeltsin, Yekaterinburg, Russia*

<sup>c</sup> *Institute of Solid State Chemistry, Ural Branch, Russian Academy of Sciences, Yekaterinburg, Russia*

<sup>d</sup> *NPAG, Faculty of Engineering and Environment, Northumbria University, Ellison Place, Newcastle upon Tyne NE1 8ST, UK*

<sup>e</sup> *Scientific-Practical Material Research Centre, National Academy of Belarus, Minsk, Belarus*

<sup>f</sup> *Department of Material Science, Tallinn University of Technology, Tallinn, Estonia*

<sup>g</sup> *Department of Physics, SUPA, University of Strathclyde, G4 0NG Glasgow, UK*

\* *e-mail: sulimov.m.a@gmail.com*

Received December 4, 2018; accepted December 5, 2018

**Abstract**— $\text{Cu}_2\text{ZnSnSe}_4$  (CZTSe) is amongst leading candidates for the absorber layer in sustainable solar cells. We examine CZTSe thin films with  $[\text{Cu}]/[\text{Zn} + \text{Sn}]$  of 0.99 and  $[\text{Zn}]/[\text{Sn}]$  of 1.07, deposited on Mo/glass substrates, and solar cells fabricated from these films. The bandgap ( $E_g$ ) of the as deposited films and solar cells was examined by photoluminescence excitation (PLE) whereas the temperature and excitation intensity dependence of photoluminescence (PL) spectra was used to examine the nature of radiative recombination. The 6 K PL spectra of CZTSe/Mo exhibit an intense broad and asymmetrical band P1 at 0.822 eV and a lower intensity band P2 at 0.93 eV. The shape of this band, high rates of blue shift with excitation intensity rise ( $j$ -shift)  $j(\text{P1}) = 14$  meV and  $j(\text{P2}) = 8$  meV per decade, and red shifts of both bands with increasing temperature suggest that both bands are associated with valence band tails due to potential fluctuations caused by high populations of charged defects. The mean depth of such fluctuation  $\gamma$  of 24 meV was estimated from the low energy side of P1. Device processing increased  $E_g$ , blue shifted P1, decreased its width,  $j$ -shift and the mean depth of potential fluctuations. These can be due to the annealing and/or can partly be related to KCN etching and the chemical effect of Cd, from CdS replacing copper at the CdS–CZTSe interface layer. Processing induced a new broad band P3 at 1.3 eV (quenching with  $E_a = 200$  meV). We attributed P3 to defects in the CdS layer.

DOI: 10.1134/S1063783419050214

### 1. INTRODUCTION

$\text{Cu}_2\text{ZnSnSe}_4$  (CZTSe) is a further development of  $\text{Cu}(\text{In,Ga})\text{Se}_2$  (CIGS). CIGS is used as the absorber layer of solar cells [1] which have a leading record conversion efficiency  $\eta$  amongst thin film photovoltaic (PV) devices. CZTSe-based laboratory size cells achieved  $\eta$  of 11.6% [2] demonstrating a high potential of such technology for sustainable PV devices employing low cost and toxicity elements abundant in the earth's crust. An efficient  $p$ -type doping of CZTSe can be achieved by intrinsic defects generated by shifting the elemental composition towards significant Cu deficiency and Zn excess [3]. The Cu-based defect copper vacancy  $V_{\text{Cu}}$  is believed to be the dominant acceptor. However high  $\eta$  can also be achieved for CZTSe with near stoichiometric copper contents [4]. Although a decrease of  $[\text{Cu}]/[\text{Zn} + \text{Sn}]$  in this study

improved the solar cell efficiency up to 8.1% there are other reports demonstrating a deterioration of the efficiency with decreasing  $[\text{Cu}]/[\text{Zn} + \text{Sn}]$  [5, 6]. These suggest that the model proposed in [3] might only be valid for a limited range of CZTSe fabrication technologies whereas the defect chemistry in CZTSe is generally more complex with near stoichiometric copper content material having much potential as the absorber layer in high performance solar cells.

To improve the performance of solar cells with near stoichiometric  $[\text{Cu}]/[\text{Zn} + \text{Sn}]$  ratios of CZTSe one have to gain more experimental data about the defect chemistry of such CZTSe thin films and understand the influence of solar cell processing steps required for the fabrication of solar cells. Optical spectroscopy is an efficient tool to gain experimental information on defects in semiconductors.

Photoluminescence (PL) is a useful characterisation technique to analyse the electronic properties of semiconductors [7]. Low temperature PL spectra of device quality CZTSe are dominated by a broad emission band that is assigned to band-tail related recombination mechanisms [8–10]. The spectral position of such a band depends on a number of factors: the bandgap  $E_g$ , that is influenced by the degree of Cu/Zn disorder [11, 12], the mean depth of the band tail as well as the type of the tail-related radiative recombination [4], the energy level of the defect [13], as well as the sample temperature and excitation intensity [4, 9, 10]. It follows that accurate interpretation of PL spectra requires measurement of the bandgap. In non-transparent CZTSe films deposited on Mo/glass substrates  $E_g$  can be determined using photoluminescence excitation (PLE) spectroscopy [4, 10].

In this paper we present a detailed optical spectroscopy study of CZTSe thin films (with a near stoichiometric copper content) deposited on Mo/glass substrates and explore the influence of solar cell processing steps (KCN etching, deposition of CdS and ZnO) on the PL and PLE spectra.

## 2. EXPERIMENTAL

Solar cells with  $\eta$  of 6.4% were produced from CZTSe thin films on Mo/glass substrates by the selenisation of metallic precursors.

Molybdenum layers with a thickness of 0.85  $\mu\text{m}$  were deposited on soda-lime glass substrates using magnetron sputtering. Multilayer metallic precursors, constituting a few nanometres thick alternating copper, zinc and tin layers, were sequentially deposited on the Mo-coated glass substrates (held on a rotating table) by three-target magnetron sputtering of high-purity (5N) elemental metal targets at room temperature. These precursors were then selenised in a mixture of selenium vapour with argon using a two-stage thermal annealing process. This involved heating to 300°C for 5 min and then to 500°C for 15 min.

The CdS buffer layer was deposited using a standard chemical bath process at 70°C following a 0.5 min etch of the films in a 10 wt % KCN solution [14]. Solar cells with an area of  $3 \times 3 \text{ mm}^2$  were then fabricated by DC-magnetron deposition of ZnO/ZnO:Al transparent front contacts and mechanical scribing.

The solar cell parameters were measured under standard test conditions (25°C, AM1.5 and 100  $\text{mW}/\text{cm}^2$ ). The current density versus voltage parameters ( $J-V$ ) were measured by directly contacting the solar cell front surface without any deposited metallic grid. The solar cells, fabricated using the films, demonstrated a conversion efficiency of 6.4% along with an open circuit voltage  $V_{oc} = 374 \text{ mV}$ , short circuit current density  $J_{sc} = 29.7 \text{ mA cm}^{-2}$  and fill factor  $FF = 56.3\%$ . More

information on the deposition process and solar cell characterisation can be found elsewhere [4, 10, 14].

A 100 cm single grating monochromator and the unfocused 514 nm line (0.7 mm diameter) of a 300 mW  $\text{Ar}^+$  laser were used for the PL measurements. For the PLE measurements two single grating monochromators, with focal lengths of 60 and 30 cm, were used to register the signal and for a tuneable source of light from a 400 W halogen lamp, respectively. The PLE spectra were measured by detecting the signal at the energy of the dominant PL band (0.8 eV). An InGaAs photomultiplier tube sensitive from 0.9 to 1.7  $\mu\text{m}$  was used to detect the PL signal. A closed-cycle helium cryostat was used to measure the temperature dependence of the PL spectra (from 6 to 300 K). The PLE measurements were carried out at 4.2 K using a liquid helium bath cryostat. More experimental details can be found in [4, 10].

The morphology of the bare CZTSe films was examined by scanning electron microscopy (SEM) using a 5 keV electron beam energy. Wavelength dispersive X-ray (WDX) microanalysis was performed at a 10 keV electron beam energy.

## 3. RESULTS AND DISCUSSION

### 3.1. Results

A dense film with the grain size in excess of 1  $\mu\text{m}$  can be seen in a SEM cross section micrograph in Fig. 1. The film average thickness of 1.2  $\mu\text{m}$  can be estimated from the view. The WDX measurements have been taken at 10 points along a line of 1 mm. The elemental composition (Cu 25.6, Zn 13.3, Sn 12.5 and Se 48.6 at %) demonstrates a near stoichiometric ratio of copper to other metals  $[\text{Cu}]/[\text{Zn} + \text{Sn}] = 0.99 \pm 0.02$ , an excess of zinc over tin  $[\text{Zn}]/[\text{Sn}] = 1.07 \pm 0.03$  and a slightly selenium deficiency, the ratio of Se to the sum of metals  $[\text{Se}]/[\text{Cu} + \text{Zn} + \text{Sn}] = 0.94 \pm 0.01$ . The standard deviations of the 10 measurements are taken as the error bars.

A comparison of the PL spectra (measured at 6 K and excitation power density of 0.32  $\text{W}/\text{cm}^2$ ) from the CZTSe/Mo/glass with that of the solar cell is shown in Fig. 2a on a logarithmic scale. Device processing reduces the intensity of the P1 band by a factor of 2.5 whereas that of the P2 band increases by a factor of 1.5. Also, processing induces a very broad and low intensity P3 band. Its maximum intensity was observed at the verge of the detector sensitivity limit of 1.3 eV.

The PL spectra, taken at different points across the surface, reveal similar intensities as well as shapes of the P1, P2 and P3 bands demonstrating homogeneity of the films on a macroscale.

Figure 2b shows the P1 band in the PL spectra of CZTSe/Mo and solar cell on a linear scale after normalisation. It can be seen that processing blue shifts the P1 band from 0.812 eV before to 0.822 eV after whereas the full width at half maximum (FWHM) of

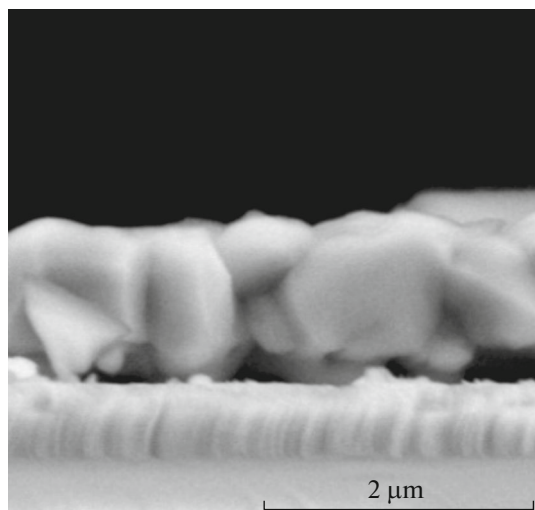


**Fig. 1.** A cross-section SEM micrograph of the CZTSe film on Mo/glass substrate.

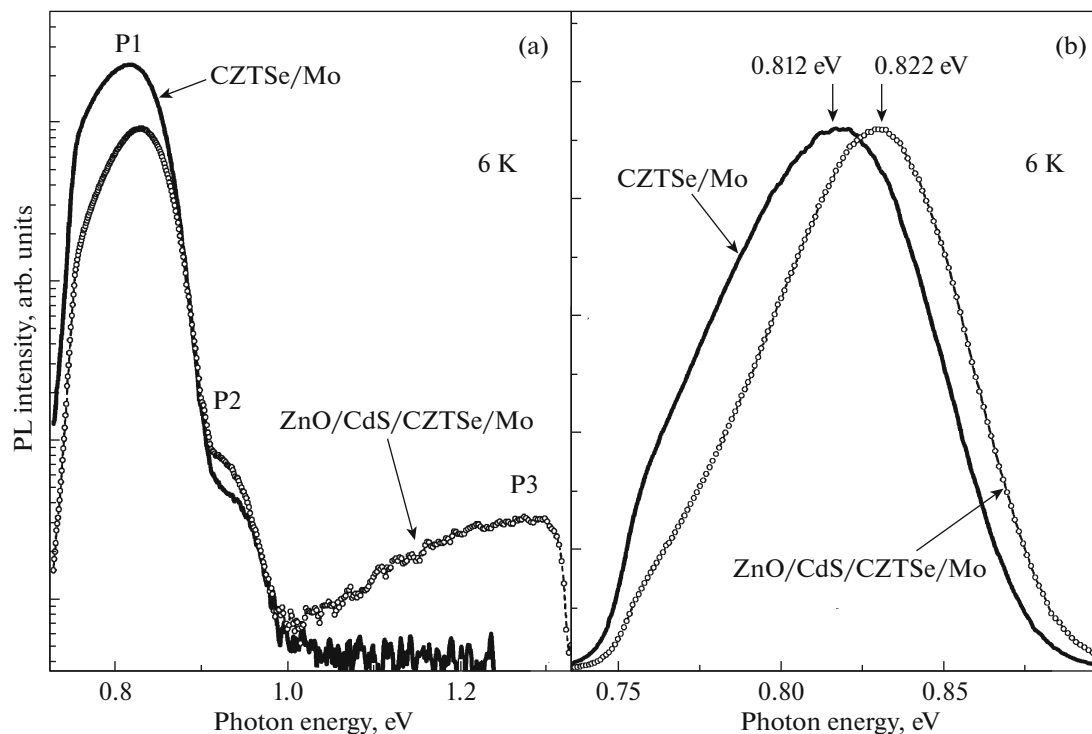
the P1 band decreases after the processing from 84 to 76 meV. The linear scale of the PL spectra in Fig. 2b brings out the asymmetrical shape of the P1 band. In both spectra one can see a rather steep high energy side and a gentler low energy one. The dependence of the PL spectra on the laser excitation intensity is shown in Fig. 3. Increasing laser power induces significant blue

shifts in the spectral position of the P1 band in both CZTSe/Mo (a) and the solar cell (b) whereas their shape does not change. The rate of this shift ( $j$ -shift) is 14 meV per decade of laser power change for the CZTSe/Mo film and decreases to 13 meV/d for the cell spectra as shown in Table 1.

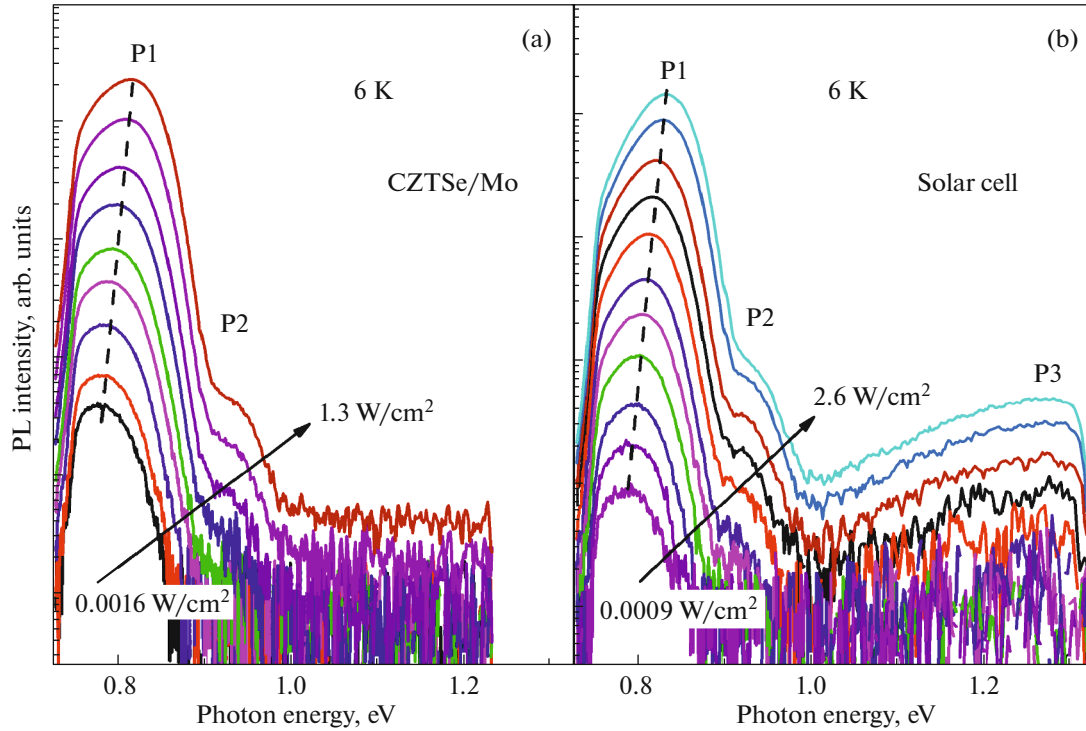
The characteristic asymmetric shape of the P1 band, the invariance of this shape on the excitation intensity and the significant  $j$ -shifts suggest that the radiative recombination mechanism of this band is associated with band tails generated by spatial potential fluctuations due to high concentrations of charged defects [8, 10, 15–17].

Figure 4 shows the temperature dependence of the PL spectra. It can be seen at Fig. 4b that the P1 band red shifts up to a temperature of 70 K and then at higher temperatures it reveals a blue shift. In the chalcopyrites [17] and kesterites [4, 8, 10, 15] similar temperature dependencies were taken as evidence of the band-tail related nature of such transitions. As in the film the P2 band quenches by 70 K. At temperatures above 200 K the solar cell spectra show a broad band at 0.9 eV. Such bands, observed earlier in CZTS [18] and CZTSe [4, 10, 15], were attributed to band-to-band (BB) transitions, involving the recombination of free electrons from the conduction band with free holes from the valence band.

High concentrations of charged defects generate tails in the density of states (DOS) of the conduction



**Fig. 2.** A comparison of the PL spectra of CZTSe/Mo before and after device processing on a logarithmic scale (a) and on a linear scale after normalisation of P1 band (b).



**Fig. 3.** Excitation intensity dependencies of the PL spectra in CZTSe/Mo/glass (a) and the solar cell (b) measured at 6 K.

and valence bands of semiconductors. Such tails can be induced by spatial potential fluctuations [16, 17] and/or by fluctuations of the bandgap [19].

**Table 1.** Spectral positions  $E_{\max}$ , FWHM,  $j$ -shift of the P1 and P2 PL bands at 6 K and an excitation intensity of  $0.8 \text{ W/cm}^2$ , bandgaps  $E_g$  at 4.2 K, the broadening energies  $\Delta E$ , average depths of potential fluctuations  $\gamma$ , and activation energies  $E_a$  of the temperature quenching for CZTSe/Mo and cell

Optical parameters	CZTSe/Mo	Cell
Band	P1	P1
$E_{\max}$ (eV)	0.812	0.822
FWHM (meV)	84	76
$j$ -shift (meV/d)	14	13
$k$	1.0	1.0
$E_g$ (eV)	0.96	0.99
$\Delta E$ (meV)	33	36
$\gamma$ (meV)	24	22
$E_a$ (meV)	$65 \pm 3$	$85 \pm 5$
Band	P2	P2
$E_{\max}$ (eV)	0.936	0.928
FWHM (meV)	53	50
$j$ -shift (meV/d)	8	12
$k$	1.00	0.85
$E_a$ (meV)	$85 \pm 3$	$75 \pm 7$

A theory of the influence of spatial potential fluctuations on the electronic properties of semiconductors [20] has been adopted to analyse PL spectra [16]. Such analysis was successfully used to interpret PL spectra of the chalcopyrites [17] and kesterites [8]. It suggests that the characteristic asymmetric shape of the PL bands, their strong blue shift rate with increasing excitation intensity and the significant red shift with rising temperature, as observed in our PL spectra, are evidence of spatial potential fluctuations being the origin of the band tails in these spectra. Time resolved analysis of the PL emission of CZTSe [21] also suggests a potential fluctuation origin of the band tails in this material. Although we cannot totally exclude the influence of bandgap fluctuations on the formation of band-tails to interpret our results we assume the spatial potential fluctuation model [16, 17].

Thin films of CZTSe used in high performance solar cells are generally considered to have high concentrations of both donors and acceptors [4, 8, 10, 21, 22]. A semiconductor is highly doped if the mean distance between defects is smaller than their Bohr radii [20]. In the kesterites this condition can be satisfied more easily for electrons than for holes [23] because the theoretically estimated DOS mass of electrons  $m_e^* = 0.08m_0$ , whereas that of holes is greater  $m_h^* = 0.21m_0$  [24]. Overlapping donor wave-functions degenerates the material in terms of donors whereas heavy holes can stay localised either at the states of the

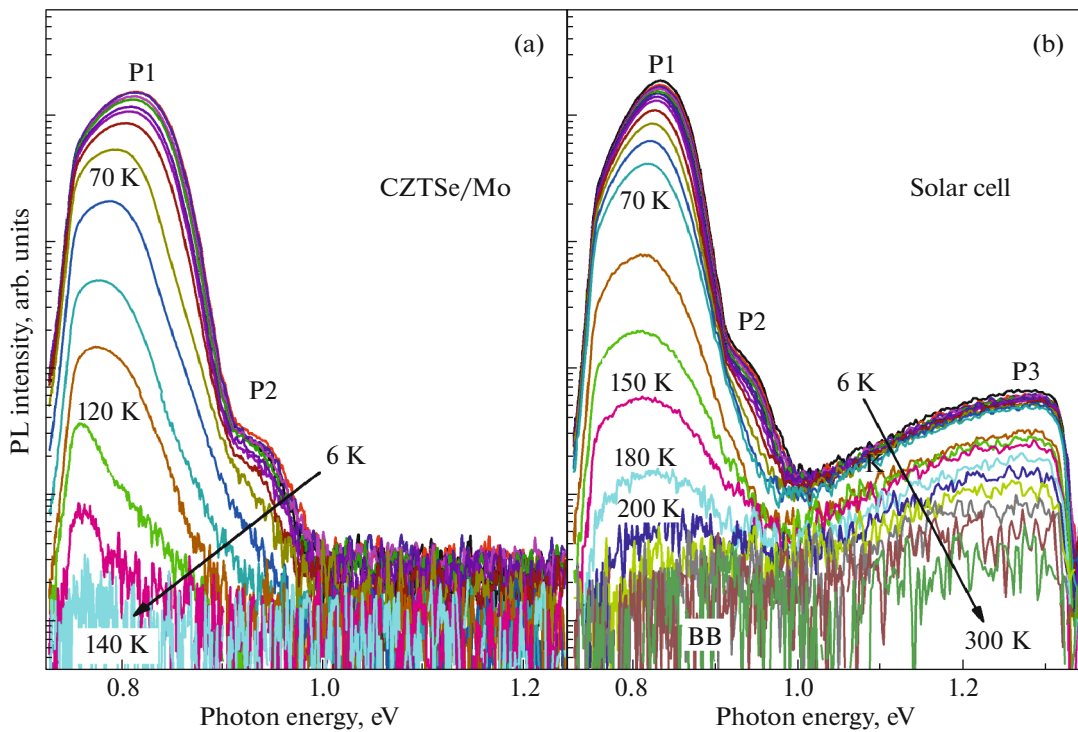


Fig. 4. The temperature dependence of the PL spectra from CZTSe/Mo/glass (a) and solar cell (b).

valence band tail or at acceptors which are deeper than the potential fluctuations [16, 17].

PLE spectra were measured for both samples to determine the bandgap. These spectra are shown in Fig. 5 along with the PL spectra. The low energy side of the PLE spectra represents the absorbance  $\alpha(E)$ . To determine  $E_g$  this side has been fitted with sigmoidal functions proposed in [25]:

$$\alpha(h\nu) = \alpha_0 / [1 + \exp(E_g - h\nu) / \Delta E], \quad (1)$$

where  $h\nu$  represents the photon energy,  $\alpha_0$  a scaling parameter and  $\Delta E$  is a broadening parameter [26].

The best fitted curves are shown in Fig. 5 by solid lines. The determined bandgap values are  $(0.96 \pm 0.01)$  eV for CZTSe/Mo and  $(0.99 \pm 0.01)$  eV for the solar cell, respectively, as listed in Table 1. The processing has induced a considerable increase of the bandgap by 30 meV which is also accompanied by an increase of the broadening parameter from 33 to 36 meV.

### 3.2. Analysis of PL Spectra

The possible transitions which can be found in low temperature PL spectra of highly doped semiconductors, where holes are much heavier than electrons, [16, 17] are: (1) the band-to-tail (BT) recombination of holes localised at the tail of the valence band and acting like an acceptor state, with free electrons from the conduction band, (2) free-to-bound (FB) recombination of free electrons with holes localised at an accep-

tor with its energy level deeper than the mean depth of the band-tail.

On a microscale the spectral energy of such a level follows spatial fluctuations of the valence band so the spectral shape of such a FB band is similar to that of the BT one [26]. Such recombination bands have broad and asymmetric characteristic shapes, high  $j$ -shift and demonstrate characteristic red shift at increasing temperatures.

To analyse the excitation intensity and temperature dependency of the P1, P2 and P3 bands the experimental spectra were fitted with the empirical double sigmoidal functions (DSF) proposed in [17] for BT and FB bands:

$$I(h\nu) = A \left\{ 1 + \exp \left[ -\frac{(h\nu - E_1)}{W_1} \right] \right\}^{-1} \times \left\{ 1 - \left( 1 + \exp \left[ -\frac{(h\nu - E_2)}{W_2} \right] \right)^{-1} \right\}, \quad (2)$$

where  $A$ ,  $E_1$ ,  $E_2$ ,  $W_1$  and  $W_2$  are fitting parameters.  $E_1$  and  $W_1$  describe the low energy side of the band whereas  $E_2$  and  $W_2$  are associated with the high energy one. Examples of fitting of the PL spectra measured at 6 K are shown in Fig. 6 demonstrating that the fitted DSF describe the band shape well.

DSF fitting was used to decompose the P1, P2 and P3 bands from the PL spectra in order to analyse separately their temperature and excitation intensity

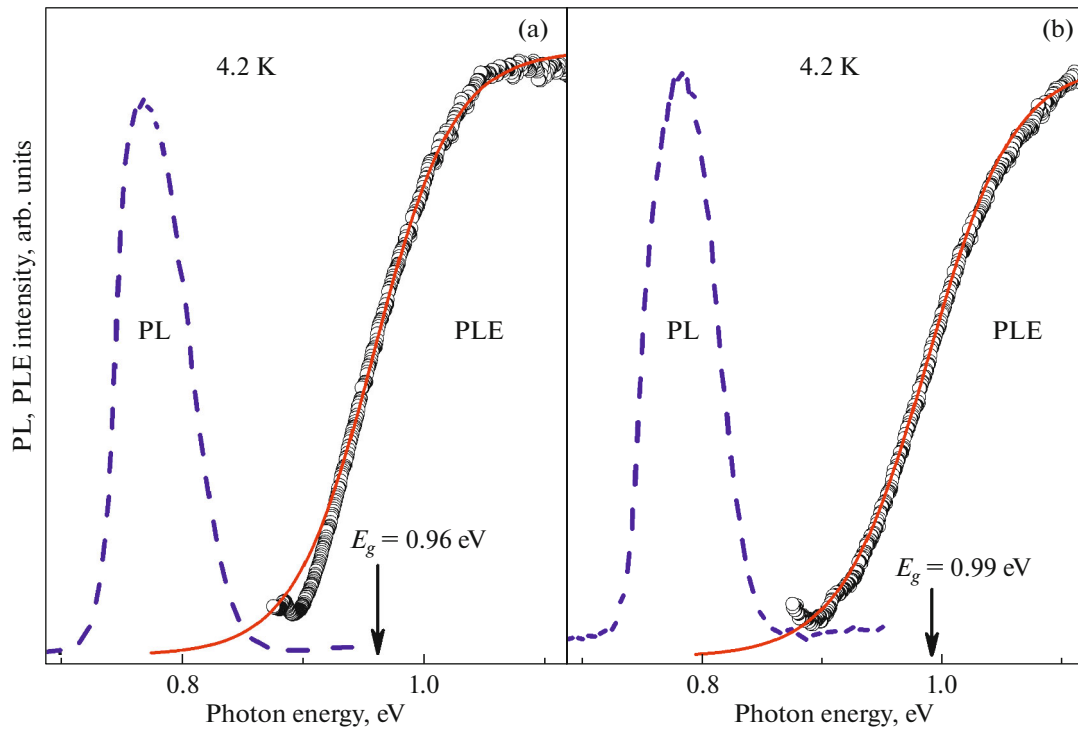


**Fig. 5.** PLE spectra (measured at the maximum of the PL bands) of CZTSe/Mo (a), cell (b) fitted (solid lines) with sigmoidal functions.

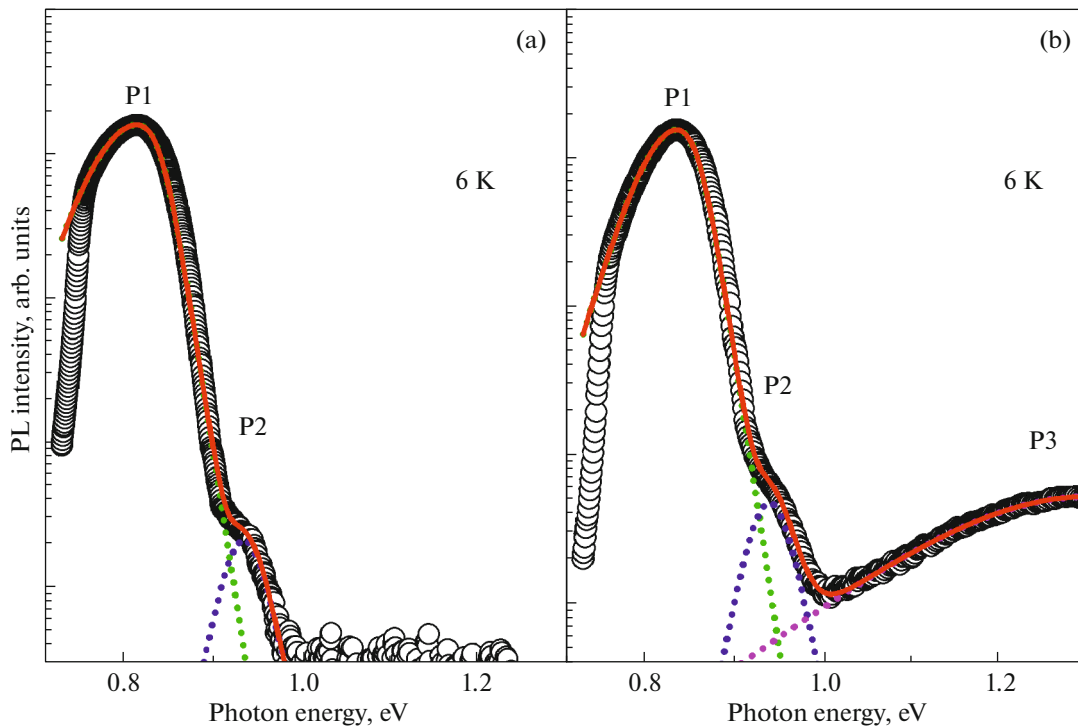


**Fig. 6.** Experimental PL spectra (symbols) of CZTSe/Mo (a) and cell (b) taken at 6 K, fitted by DSF functions (red solid lines). The P1, P2, and P3 bands are fitted by the green, blue and magenta dotted lines, respectively.

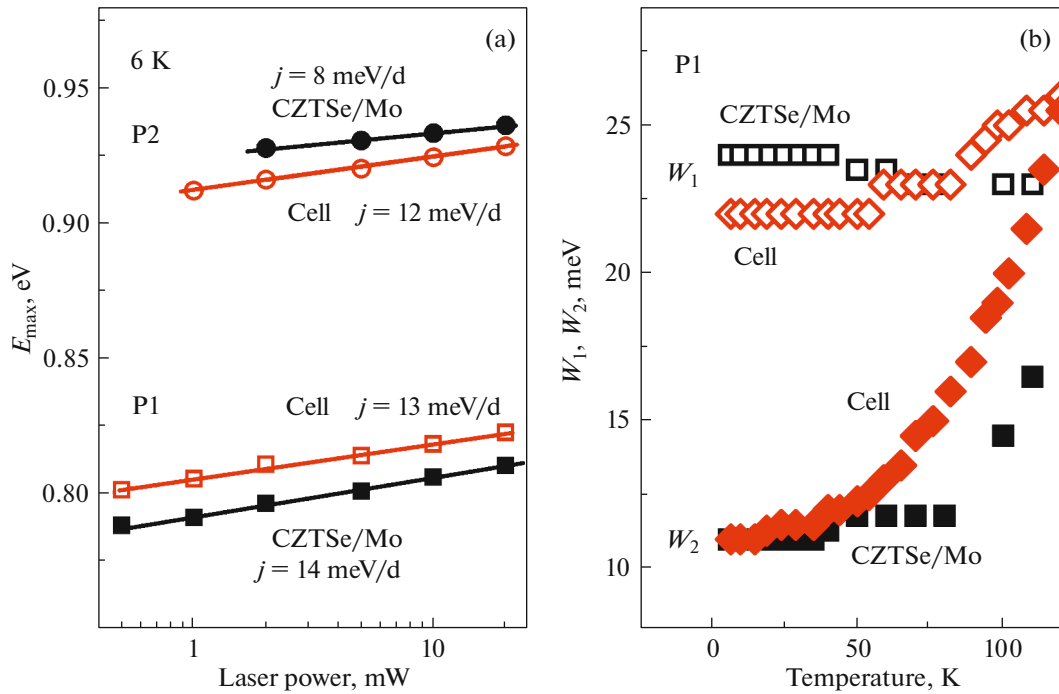


**Fig. 7.** The dependence of spectral position  $E_{\max}$  of the P1 (filled squares—CZTSe/Mo, opened squares—cell) and P2 (filled circles—CZTSe/Mo, opened circles—cell) on the excitation intensity (a), the temperature dependence of  $W_1$  and  $W_2$  for the P1 bands in the PL spectra CZTSe/Mo ( $W_1$ —open squares,  $W_2$ —filled squares) and cell ( $W_1$ —open rhombi,  $W_2$ —filled rhombi) (b).

dependence. Such decompositions helped to estimate the spectral position of the P2 band. At 0.4 W/cm<sup>2</sup> laser excitation power density this was at 0.936 eV for CZTSe/Mo and 0.928 eV for the cell, with the FWHM at 53 and 50 meV, respectively.

The decomposition of P1 and P2 provides an opportunity to estimate the intensity of P2 and to compare it with that of P1. Before solar cell processing the P1 band intensity exceeded that of P2 by a factor of 600, whereas after processing, the intensity of P1 decreases and that of P2 increases, reducing the intensity ratio to about 140. A comparison of the  $j$ -shifts for the P1 and P2 bands is shown in Fig. 7a. The dependence of the integrated intensity  $I$  of a PL band on excitation laser power  $P$  can be described as  $I(P) \sim P^k$ , where  $k$  is a coefficient which can be determined from the gradient of a straight line fitted to a  $\log(I)$ – $\log(P)$  scale. For both P1 and P2 bands in the CZTSe/Mo spectra the  $k$  value is found to be of 1.0. The processing does not change  $k$  for the P1 band whereas for P2 it reduced  $k$  to 0.85 as shown in Table 1. According to [27] the presence of defect energy levels within the bandgap results in the involvement of these defects in radiative recombination processes reducing  $k$ -values below unity whereas  $k$  values greater than unity, should be taken as an indication of transitions not involving defects. A near unity value of  $k$  could be due to the presence of an unresolved BB recombination in the dominant band. The BB transition was reported in

the PL spectra of CZTSe from cryogenic temperatures up to 300 K [4, 10, 15].

The low-energy sides of the bands are determined by the density of states (DOS) of the valence band tail  $\rho_v$  [16, 17, 22] which in the case of the BT transition can be described at low temperatures by the following function:

$$\rho_v(\epsilon) \sim \exp(-\epsilon/\gamma), \quad (3)$$

where  $\gamma$  is the average energy depth of the spatial potential fluctuations in the valence band and  $\epsilon$  is the energy from the valence band top. The FB transition is associated with the recombination of free electrons with holes localised directly at the acceptor as well as holes first localised at the valence band tail states, released and then captured at the acceptor. Potential fluctuations spread the acceptor's level to a band with a Gaussian distribution [16, 22, 28] so the hole density of states can be described as:

$$\rho_a(\epsilon) = (N_a/\sqrt{2\pi}\gamma) \exp[-(\epsilon - I_a)^2/2\gamma^2], \quad (4)$$

where the acceptor ionisation energy is  $I_a$  and  $N_a$  is the acceptor concentration. Thus, in both cases spatial potential fluctuations determine the low energy side of the band and its shape can be used to determine the average depth of potential fluctuations  $\gamma$ . To identify which of the recombination mechanisms is more likely to be present in our spectra we examine the temperature quenching of the band to find activation energies

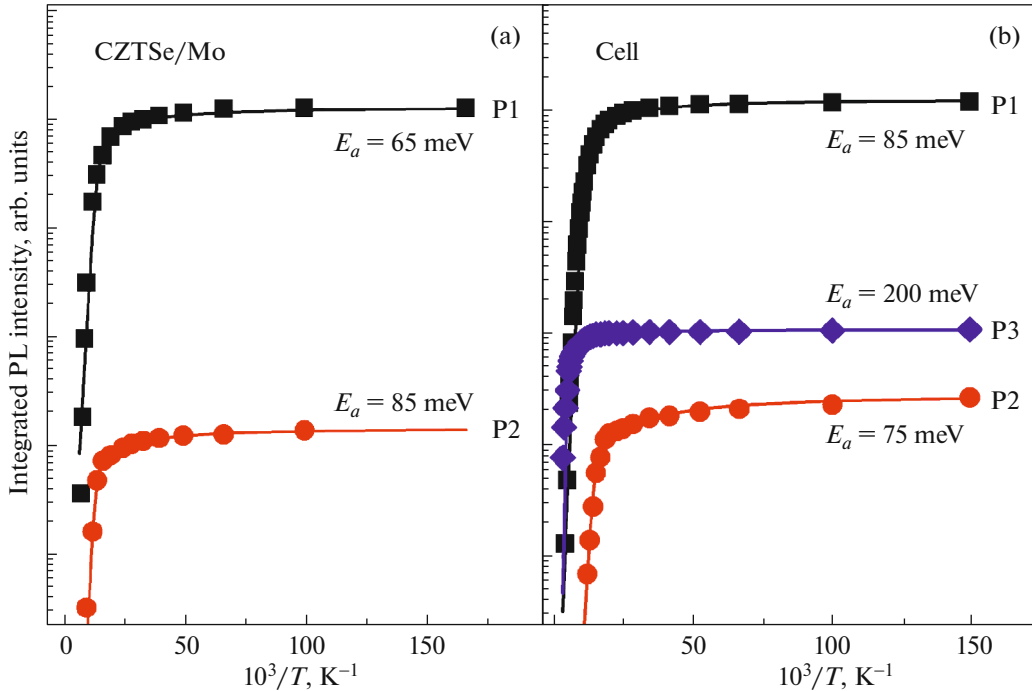


Fig. 8. Arrhenius plots fitted to the integrated intensities of the bands in the PL spectra of CZTSe/Mo (a) and cell (b).

and compare them with  $\gamma$ . In the case when the activation energy is a fraction of  $\gamma$  the band can be assigned to the BT transition. If the activation energy is greater than  $\gamma$  then the band should be attributed to FB. The  $W_1$  and  $W_2$  temperature dependence of the CZTSe/Mo film and the cell are shown in Fig. 7b. Up to about 50 K,  $W_1$  does not change much whereas  $W_2$  gradually rises, therefore by temperatures of 100 K the P1 band becomes more symmetrical. Its shape becomes close to Gaussian due to rising scattering of the carrier by phonons [16]. The value of  $W_1$  at low temperatures can be taken as an estimate of  $\gamma$  [17] which for CZTSe/Mo is of 24 meV whereas for the cell it is of 21 meV demonstrating a slight decrease of  $\gamma$  due to the processing. These values are shown in Table 1.

Arrhenius analysis of the temperature quenching of the P1, P2 and P3 bands was carried out assuming a single recombination channel and a dependence of the hole capture cross section on temperature [29]:

$$I(T) = I_0/[1 + A_1 T^{3/2} + A_2 T^{3/2} \exp(-E_a/k_B T)], \quad (5)$$

where for the intensity of the analysed band  $I$  we used the integrated intensity of P1, P2 and P3. The band intensity at the lowest used temperature (6 K) is  $I_0$ , the process rate parameters are  $A_1$  and  $A_2$ , and  $E_a$  is the process activation energy. Arrhenius fits to the experimental data points for CZTSe/Mo and the cell are shown in Fig. 8. The activation energies are shown in Table 1 and are all greater than  $\gamma$ , implying that the P1 band is likely to be associated with the FB transition, the recombination of free electrons with holes local-

ised at an acceptor with the energy level influenced by spatial potential fluctuations.

### 3.3. Discussion

The reported spectral position of the dominant band in the low temperature PL spectra of CZTSe varies from 0.8 to 0.99 eV [4, 5, 8–11, 15]. This position is determined by the type of PL transition and the bandgap which in turn is influenced by the degree of Cu/Zn disorder [5, 11, 15]. Copper vacancies can suppress the disorder [30] whereas low concentration of  $V_{\text{Cu}}$ , as expected for near stoichiometric copper content, induces a high degree of the Cu/Zn disorder. At high copper contents and an excess of zinc over tin the formation of  $\text{Zn}_{\text{Cu}} + \text{Cu}_{\text{Zn}}$  antisite defect complexes is expected. According to theoretical studies [3, 31] this should result in a reduction of the bandgap. Indeed, before processing the dominant P1 band, is at about 0.81 eV in the low temperature PL spectra, whereas  $E_g$  is closer to 0.96 eV. Both values suggest a high degree of Cu/Zn disorder [12] whereas the P2 band has its spectral position blue shifted with respect to P1 by about 0.12 eV. This is consistent with a low degree of Cu/Zn disorder. The Cu/Zn disorder can be controlled by low temperature annealing reversibly changing  $E_a$  by up to 100 meV [12].

A study of CZTSe/Mo films with similar near stoichiometric  $[\text{Cu}]/[\text{Zn} + \text{Sn}]$  and excess  $[\text{Zn}]/[\text{Sn}]$  ratios demonstrated similar low temperature PL spectra with two bands: a dominant band at 0.83 eV and a

low intensity one at 0.93 eV [4]. In that report the 0.83 eV band was assigned to a high degree of Zn/Cu disorder whereas the 0.93 eV band was attributed to the presence of a small fraction of CZTSe with higher degree of ordering.

The above model was used to interpret the origin of P2 in our spectra. We assumed that due to the near stoichiometric copper content and excess of zinc, the CZTSe in our films has a high degree of Cu/Zn disorder resulting in a relatively small bandgap of 0.96 eV and the P1 dominant band at 0.812 eV. However, a fraction of the CZTSe, responsible for the P2 band, has a high degree of ordering, and a larger bandgap value. The lower intensity of this band with respect to P1 (by a factor of 600) is consistent with this fraction being rather small and, therefore, PLE measurements were not reliable for the determination of its  $E_g$ . The similarity of the PL spectra at different points demonstrates the macroscale homogeneity of the films whereas on a microscopic scale the films might contain areas with a higher degree of the Cu/Zn ordering.

Processing increased the bandgap by 30 meV. Such an increase is consistent with an improvement of the degree of the Cu/Zn order in the fraction of CZTSe generating P1 and can be induced by the annealing as observed in [12]. Once the fraction of the CZTSe with a low degree of order becomes smaller, the intensity of P1 also becomes smaller. On the other hand, an increase of the fraction of the CZTSe with a higher degree of Cu/Zn order results in a higher intensity of P2. Although the disordered CZTSe still dominates the film, the ratio of the P1 to P2 intensities becomes smaller (140).

The observed increase in  $E_g$  (by 30 meV) is expected to induce a similar blue shift to the PL bands. Indeed, the P1 band has blue shifted. However, the shift of 10 meV is significantly smaller than the increase of  $E_g$ . The P1 band was assigned to the recombination of free electrons with holes localised at an acceptor. Before device processing the acceptor had a value of  $E_a$  of 65 meV, whereas after processing,  $E_a$  became 85 meV implying a change of the acceptor for one which is about 20 meV deeper. Processing also red shifted the P2 band by about 10 meV. This was accompanied by a decrease in its activation energy from 85 to 75 meV also implying a change of the main acceptor to one which is shallower and consistent with the red shift of P2. There is a possibility that such a change in the acceptor nature has a chemical origin: cadmium atoms diffuse into CZTSe changing the chemistry of defects at the CdS/CZTSe interface layer [32]. A theoretical study of the formation energy of the CdCu antisite defects in CZTSe demonstrates that their formation energy is small although it is positive [33]. The inter-diffusion of elements at the CdS–CZTS interface takes place within a thin interface layer whereas the rest of CZTSe is not affected by Cd. This could be a reason why the observed changes in the  $j$ -values after

the processing were relatively small. It is speculated that the greater change in the  $j$ -shift of the P2 band after the processing, increasing from 8 to 12 meV/d, could be due to local copper deficiency on a micro-scale resulting in a higher degree of Zn/Cu order and responsible for P2.

The deposition of  $n$ -type CdS on  $p$ -type CZTSe forms a  $p$ – $n$  junction creating in CZTSe a space charge layer (SCL). Its thickness can be estimated as 0.3  $\mu\text{m}$  [34]. At an absorption coefficient of  $5 \times 10^4 \text{ cm}^{-1}$  [35] the thickness of the layer excited by the laser can be taken as 0.2  $\mu\text{m}$  suggesting that SCL can influence the PL emission in the cells. Under the open circuit conditions of the PL measurements the photo-injected charge carriers can significantly reduce both the thickness of SCL and the magnitude of the electric field in it [36]. The action of these charge carriers is equivalent to a forward bias distorting the equilibrium electric fields. Therefore, the influence of the  $p$ – $n$  junction on the PL spectra might be insignificant. This is supported by the similarity of the  $k$ -parameter of the dominant band P1 before and after the processing.

Device processing also induced a new broad band at 1.3 eV, quenching with  $E_a$  of 200 meV. This band was attributed to defects in the CdS layer.

#### 4. CONCLUSIONS

CZTSe thin films with a near stoichiometric [Cu]/[Zn + Sn] ratio, fabricated on Mo/glass substrates by the selenisation of metallic precursors, were processed to produce solar cells ( $V_{oc} = 374 \text{ mV}$ ,  $J_{sc} = 29.7 \text{ mA}$ ,  $FF = 57.7\%$ ,  $\eta = 6.4\%$ ) by a KCN etching and the deposition of CdS and ZnO layers. The low temperature PL spectra of CZTSe/Mo reveal an intense band P1 at 0.81 eV and a low intensity band P2 at 0.93 eV. A comparison of their temperature quenching activation energies with  $\gamma$  suggests that both can be attributed to the free-to-bound recombination of free electrons with holes localised at acceptors with the energy levels spread by the potential fluctuations. It is suggested that due to its inhomogeneity CZTSe contains micro-volumes with different degrees of Cu/Zn ordering on the cation sub-lattice: a large fraction with a low degree of ordering (generating P1) and a small fraction of highly ordered Cu/Zn (generating P2). Device processing increased  $E_g$  from 0.96 to 0.99 eV, blue shifted P1, decreased its width,  $j$ -shift and  $\gamma$ . However device processing also decreased the P1 intensity by a factor of 2.5 whereas that of P2 increased by a factor of 1.5. These changes suggest an improvement of the structural quality of CZTSe, which can partly be attributed to the effect of cleaning the film by KCN etching, the chemical effect of Cd diffusing from CdS and taking copper vacancies at the CdS–CZTSe interface layer, and/or low temperature annealing due to the CdS and ZnO deposition increasing the fraction

of CZTSe with a high degree of Cu/Zn ordering (raising the intensity of P2) and decreasing the fraction with a low degree of Cu/Zn ordering (reducing the intensity of P1).

### FUNDING

This research was supported by the Russian Science Foundation (grant 17-12-01500).

### REFERENCES

- X. Liu, Y. Feng, H. Cui, F. Liu, X. Hao, G. Conibeer, D. B. Mitzi, and M. Green, *Prog. Photovolt.* **24**, 879 (2016).
- Y. S. Lee, T. Gershon, O. Gunawan, T. K. Todorov, T. Gokmen, Y. Virgus, and S. Guha, *Adv. Energy Mater.* **12**, 1401372 (2015).
- S. Chen, A. Walsh, X. G. Gong, and S. H. Wei, *Adv. Mater.* **25**, 1522 (2013).
- M. V. Yakushev, M. A. Sulimov, J. Márquez-Prieto, I. Forbes, J. Krustok, P. R. Edwards, V. D. Zhivulko, O. M. Borodavchenko, A. V. Mudryi, and R. W. Martin, *Sol. Energy Mater. Sol. Cells* **168**, 69 (2017).
- M. Lang, T. Renz, N. Mathes, M. Neuwirth, T. Schnabel, H. Kalt, and M. Hetterich, *Appl. Phys. Lett.* **109**, 142103 (2016).
- O. Demircioğlu, J. F. L. Salas, G. Rey, T. Weiss, M. Mousel, A. Redinger, S. Siebentritt, J. Parisi, and L. Gütay, *Opt. Express* **25**, 5327 (2017).
- E. W. Williams and H. B. Bebb, *Semiconductors and Semimetals* (Academic, New York, 1972).
- M. Grossberg, J. Krustok, K. Timmo, and M. Altsaar, *Thin Solid Films* **517**, 2489 (2009).
- S. Oueslati, G. Brammertz, M. Buffiere, C. Koble, T. Oualid, M. Meuris, and J. Poortmans, *Sol. Energy Mater. Sol. Cells* **134**, 340 (2015).
- J. Márquez-Prieto, M. V. Yakushev, I. Forbes, J. Krustok, V. D. Zhivulko, P. R. Edwards, M. Dimitrievska, V. Izquierdo-Roca, N. M. Pearsall, A. V. Mudryi, and R. W. Martin, *Sol. Energy Mater. Sol. Cells* **152**, 42 (2016).
- A. R. G. Rey, J. Sandler, T. P. Weiss, M. Thevenin, M. Guennou, B. El Adib, and S. Siebentritt, *Appl. Phys. Lett.* **105**, 112106 (2014).
- C. Krämmer, C. Huber, C. Zimmermann, M. Lang, T. Schnabel, T. Abzieher, E. Ahlswede, H. Kalt, and M. Hetterich, *Appl. Phys. Lett.* **105**, 262104 (2014).
- D. Tiwari, E. Skidchenko, J. W. Bowers, M. V. Yakushev, R. W. Martin, and D. J. Fermin, *J. Mater. Chem. C* **5**, 12720 (2017).
- J. Márquez, M. Neuschitzer, M. Dimitrievska, R. Gunder, S. Haass, M. Werner, Y. E. Romanyuk, S. Schorr, N. M. Pearsall, and I. Forbes, *Sol. Energy Mater. Sol. Cells* **144**, 579 (2016).
- M. V. Yakushev, J. Márquez-Prieto, I. Forbes, P. R. Edwards, V. D. Zhivulko, A. V. Mudryi, J. Krustok, and R. W. Martin, *J. Phys. D* **48**, 475109 (2015).
- A. P. Levanyuk and V. V. Osipov, *Sov. Phys. Usp.* **24**, 187 (1987).
- J. Krustok, H. Collan, M. Yakushev, and K. Hjelt, *Phys. Scr.* **79**, 179 (1999).
- M. Grossberg, P. Salu, J. Raudoja, and J. Krustok, *J. Photon. Energy* **3**, 030599 (2013).
- J. Mattheis, U. Rau, and I. H. Werner, *J. Appl. Phys.* **101**, 113519 (2007).
- B. Shklovskii and A. Efros, *Electronic Properties of Doped Semiconductors* (Springer, Berlin, 1984).
- T. Gokmen, O. Ganawan, T. K. Todorov, and D. B. Mitzi, *Appl. Phys. Lett.* **103**, 103506 (2013).
- S. Siebentritt, N. Papathanasioua, and M. Ch. Lux-Steiner, *Phys. B (Amsterdam, Neth.)* **376–377**, 831 (2006).
- J. P. Teixeira, R. A. Sousa, M. G. Sousa, A. F. Cunha, P. A. Fernandes, P. M. P. Salome, and J. P. Leitao, *Phys. Rev. B* **90**, 235202 (2014).
- C. Persson, *J. Appl. Phys.* **107**, 053710 (2010).
- K. P. O'Donnell, R. W. Martin, and P. G. Middleton, *Phys. Rev. Lett.* **82**, 237 (1999).
- M. E. White, K. P. O'Donnell, R. W. Martin, S. Pereira, C. J. Deatcher, and I. M. Watson, *Mater. Sci. Eng. B* **93**, 147 (2002).
- T. Schmidt, K. Lischka, and W. Zulehner, *Phys. Rev. B* **45**, 8989 (1992).
- A. Jagomagi, J. Krustok, J. Raudoja, M. Grossberg, M. Danilson, and M. Yakushev, *Phys. B (Amsterdam, Neth.)* **337**, 369 (2003).
- J. Krustok, H. Collan, and K. Hjelt, *J. Appl. Phys.* **81**, 1442 (1997).
- M. Paris, L. Choubrac, A. Lafond, C. Guillot-Deudon, and S. Jobic, *Inorg. Chem.* **53**, 8646 (2014).
- D. Huang and C. Persson, *Thin Solid Films* **535**, 265 (2013).
- M. Bar, I. Repins, L. Weinhardt, J.-H. Alsmeier, S. Pookpanratana, M. Blum, W. Yang, C. Heske, R. G. Wilks, and R. Noufi, *ACS Energy Lett.* **2**, 1632 (2017).
- T. Maeda, S. Nakamura, and T. Wada, *Jpn. J. Appl. Phys.* **51**, 10NC11 (2012).
- S. Ranjbar, G. Brammertz, B. Vermang, A. Hadipour, M. Sylvester, A. Mule, M. Meuris, A. F. Cunha, and J. Poortmans, *Thin Solid Films* **633**, 127 (2017).
- M. I. Amal and K. H. Kim, *Chalcogenide Lett.* **9**, 345 (2012).
- W. K. Metzger, R. K. Ahrenkiel, J. Dashdorj, and D. J. Friedman, *Phys. Rev. B* **71**, 035301 (2005).